Physica D 308 (2015) 26–33

Contents lists available at ScienceDirect

Physica D

journal homepage: www.elsevier.com/locate/physd

Transport bounds for a truncated model of Rayleigh–Bénard convection

Andre N. Souza [a], Charles R. Doering [a,b,c,*]

[a] Department of Mathematics, University of Michigan, Ann Arbor, MI 48109-1043, USA
[b] Center for the Study of Complex Systems, University of Michigan, Ann Arbor, MI 48109-1120, USA
[c] Department of Physics, University of Michigan, Ann Arbor, MI 48109-1040, USA

HIGHLIGHTS

- Analysis of a distinguished 8-mode model of Rayleigh–Bénard convection.
- New application of control techniques to upper bound theory.
- Novel insights into optimal heat transport.

ARTICLE INFO

Article history:
Received 9 November 2014
Received in revised form
12 May 2015
Accepted 23 May 2015
Available online 10 June 2015
Communicated by E.S. Titi

Keywords:
Rayleigh–Bénard convection
Lorenz equations
Heat transport
Optimal control

ABSTRACT

We investigate absolute limits on heat transport in a truncated model of Rayleigh–Bénard convection. Two complementary mathematical approaches – a background method analysis and an optimal control formulation – are used to derive upper bounds in a distinguished eight-ODE model proposed by Gluhovsky, Tong, and Agee. In the optimal control approach the flow no longer obeys an equation of motion, but is instead a control variable. Both methods produce the same estimate, but in contrast to the analogous result for the seminal three-ODE Lorenz system, the best upper bound apparently does not always correspond to an exact solution of the equations of motion.

1. Introduction

Modal truncations of partial differential equations have a long history of modeling interesting physics and producing interesting mathematics. Low dimensional dynamical systems approximations can provide insights into the full partial differential equations of motion, and they can serve as a simplified setting in which to test analytical and numerical techniques. Perhaps most notably, Bénard's turn-of-the-previous-century experiments [1] inspired Rayleigh's 1916 model [2] employing the Boussinesq approximation of the Navier–Stokes equations for buoyancy-driven flows, which subsequently lead to the celebrated Lorenz equations [3]. In the context of fluid mechanics, certain distinguished truncations, e.g., those respecting energy and/or enstrophy conservation in the inviscid limit, are of particular interest [4]. In this paper we derive rigorous limits on some time-averaged quantities for solutions of such a truncation of Rayleigh's model in order to develop and study a new optimal control approach to bounding transport – even turbulent transport – in fluid flows.

In modern dimensionless form, Rayleigh's model is

$$\partial_t \Delta\psi - J[\psi, \Delta\psi] = \sigma\Delta^2\psi + \mathrm{Ra}\,\sigma\,\partial_x\theta \tag{1}$$

$$\partial_t\theta - J[\psi,\theta] = \Delta\theta + \partial_x\psi \tag{2}$$

where $\psi(x,z,t)$ is the stream function and $\theta(x,z,t)$ is the deviation of the temperature from the linear profile of the conduction state. The Jacobian $J[f,g] = \partial_x f\partial_z g - \partial_x g\partial_z f$, and we consider the spatial domain $[0, A\pi] \times [0,\pi]$ where A is the aspect ratio. The stream function satisfies stress-free boundary conditions ($\partial_z^2\psi = 0$) and θ vanishes on the vertical (z) boundaries, and everything is periodic in the horizontal (x) direction. The parameters of the model are the Prandtl number σ, the ratio of kinematic viscosity to thermal diffusivity in the fluid, and the Rayleigh number

* Corresponding author at: Department of Physics, University of Michigan, Ann Arbor, MI 48109-1040, USA.
E-mail addresses: sandre@umich.edu (A.N. Souza), doering@umich.edu (C.R. Doering).

http://dx.doi.org/10.1016/j.physd.2015.05.009
0167-2789/

Ra, the non-dimensional gauge of the imposed temperature drop across the layer. In this formulation on this domain Ra is the "traditional" Rayleigh number divided by π^4 so that the onset of convection for $A = 2\sqrt{2}$ occurs at the minimum critical value $\mathrm{Ra}_c = \frac{27}{4}$.

We use angle brackets $\langle\cdot\rangle$ to denote the spatio-temporal average

$$\langle f\rangle = \lim_{T\longrightarrow\infty} \int_0^T \frac{dt}{T} \int_0^{A\pi} \frac{dx}{A\pi} \int_0^{\pi} \frac{dz}{\pi} f(x,z,t), \tag{3}$$

assuming that the long time limit exists. Then the nondimensional measure of heat transport is the Nusselt number

$$\mathrm{Nu} = 1 + \langle\theta\partial_x\psi\rangle, \tag{4}$$

and the flow intensity is indicated by the Péclet number Pe which for our purposes is the root mean square vorticity (i.e., the square root of the enstrophy, which is itself proportional to the bulk viscous energy dissipation rate):

$$\mathrm{Pe} = \langle(\Delta\psi)^2\rangle^{1/2}. \tag{5}$$

The Péclet and Nusselt number are related by

$$\mathrm{Pe}^2 = \mathrm{Ra}(\mathrm{Nu}-1), \tag{6}$$

derived by multiplying (1) by ψ and taking the spatio-temporal average employing suitable integrations by parts utilizing the boundary conditions.

Finite dimensional dynamical systems are naturally derived as Galerkin truncations of the Boussinesq equations, but only a subset of such truncations preserves certain physical features of the full system. For example the seven-ODE model of Thiffeault [5] conserves energy in the inviscid limit. The truncation we focus on in this paper is the eight-ODE model of Gluhovsky et al. [6], an extension of the seven-ODE system that includes an extra shear mode to conserve enstrophy in the dissipationless limit as well. Recent research revealed that this eight-ODE model captures many more details of the bifurcation structure of Rayleigh's model near onset [7]. Henceforth we refer to the eight-ODE system as the Double Lorenz Equations for reasons that will be clear momentarily.

The Double Lorenz Equations [6] emerge from the Galerkin truncation

$$\begin{aligned}\psi(x,z,t) &\approx 2\frac{1+k^2}{\sqrt{2}k}x_1(t)\sin(kx)\sin(z) + \frac{4+k^2}{\sqrt{2}k}x_2(t)\cos(kx)\sin(2z)\\ &\quad + 2\frac{1+k^2}{k}w_1(t)\sin(z) + \frac{2}{3}\frac{1+k^2}{k}w_2(t)\sin(3z)\end{aligned} \tag{7}$$

$$\begin{aligned}\theta(x,z,t) &\approx \frac{2}{\sqrt{2}}y_1(t)\cos(kx)\sin(z) + z_1(t)\sin(2z)\\ &\quad - \frac{1}{\sqrt{2}}y_2(t)\sin(kx)\sin(2z) + \frac{1}{2}z_2(t)\sin(4z),\end{aligned} \tag{8}$$

where $k = 2/A$. Rescaling time $t \mapsto (1+k^2)^{-1}t$ leads to the ordinary differential equations for the modal amplitudes

$$\dot{x}_1 = -\sigma x_1 + \sigma r_1 y_1 + (c_1 w_1 - d_1 w_2)x_2 \tag{9}$$

$$\dot{y}_1 = -y_1 + x_1 - x_1 z_1 + \frac{1}{2}(w_1 - w_2)y_2 \tag{10}$$

$$\dot{z}_1 = -b_1 z_1 + x_1 y_1 \tag{11}$$

$$\dot{x}_2 = -\sigma a x_2 + \sigma a r_2 y_2 - a(c_2 w_1 - d_2 w_2)x_1 \tag{12}$$

$$\dot{y}_2 = -a y_2 + a x_2 - a x_2 z_2 - 2(w_1 - w_2)y_1 \tag{13}$$

$$\dot{z}_2 = -b_2 a z_2 + a x_2 y_2 \tag{14}$$

$$\dot{w}_1 = -\sigma\frac{1}{4}b_1 w_1 - \frac{3}{8}a x_1 x_2 \tag{15}$$

$$\dot{w}_2 = -\sigma\frac{9}{4}b_1 w_2 + \frac{3}{8}a x_1 x_2 \tag{16}$$

where the r_i (for $i = 1, 2$) are related to the Rayleigh number and a rational function of k, and a and b_i, c_i, d_i, (also for $i = 1, 2$) are parameters that depend on k. The explicit expressions are tabulated in Appendix A. The (x_1, y_1, z_1) variables are precisely the familiar (albeit rescaled) Lorenz variables which, in this system, are coupled to a second set of Lorenz-like variables (x_2, y_2, z_2) by the shear flow modal amplitudes w_1 and w_2.

The Nusselt and Péclet numbers for the Double Lorenz Equations are obtained by inserting (7) and (8) into (4) and (5):

$$\mathrm{Nu} = 1 + \frac{1+k^2}{2}\left(\langle x_1 y_1\rangle + \frac{a}{4}\langle x_2 y_2\rangle\right), \tag{17}$$

$$\begin{aligned}\mathrm{Pe}^2 &= \frac{1}{2}\frac{(1+k^2)^4}{k^2}\langle x_1^2\rangle + \frac{1}{8}\frac{(4+k^2)^4}{k^2}\langle x_2^2\rangle + 2\frac{(1+k^2)^2}{k^2}\langle w_1^2\rangle\\ &\quad + 18\frac{(1+k^2)^2}{k^2}\langle w_2^2\rangle.\end{aligned} \tag{18}$$

The goal is to bound Nu as a function of Ra or Pe. Relation (6), which also holds for the truncated system, is used to convert between Ra and Pe.

The origin of the eight-dimensional phase space, i.e., $x_1 = x_2 = w_1 = w_2 = y_1 = y_2 = z_1 = z_2 = 0$, corresponds to the no-flow ($\mathrm{Pe} = 0$) conduction solution with $\mathrm{Nu} = 1$. This state is absolutely stable when $r_1 \le 1$ so we are generally interested in the $r_1 > 1$ regime, i.e., $\mathrm{Ra} > \mathrm{Ra}_c(k^2) = (1+k^2)^3/k^2$.

2. Background analysis

The derivation of bounds on heat transport in high Rayleigh number and turbulent convection has a long history going back more than half a century to Howard [8] and Busse [9] who formulated and scrutinized a variational formulation based on bulk power balances employing mild statistical hypothesis. Here we apply a version of the so-called "background method" [10], which does not require any statistical hypotheses, and derive upper bounds on Nu that are uniform in the Prandtl number σ. The background method has been shown to produce the same bounds as the Howard–Busse approach in some situations [11], but has also been successfully applied to prove new estimates in other cases [12,13]. It has also been employed to produce rigorous heat transport bounds for the Lorenz equations [14], some of them sharp bounds [15].

The analysis proceeds as follows. Decompose the temperature variables as $z_i(t) = z_i^0 + \varsigma_i(t)$ where z_i^0 are "background" values to be chosen later. The uniform-in-time boundedness of all the dynamical variables [6] (and Appendix B) implies

$$0 = \left\langle \frac{d}{dt}\left(y_1^2 + \varsigma_1^2 - 2z_1^0\varsigma_1 + \frac{1}{4}\left(y_2^2 + \varsigma_1^2 - 2z_2^0\varsigma_2\right)\right)\right\rangle. \tag{19}$$

(As in [15] we could take finite time averages for $t \in [0, T]$ throughout the subsequent calculations, leading to $\mathcal{O}(T^{-1})$ corrections to the formulae as $T \to \infty$, but the end result is the limit supremum of the Nusselt number being bounded by what is derived, so for simplicity of exposition we forgo the demonstration.) The equations of motion for the temperature variables equation inserted into (19) reveal

$$\begin{aligned}0 &= -\langle y_1^2\rangle - b_1\langle\varsigma_1^2\rangle + (1-2z_1^0)\langle x_1 y_1\rangle + b_1(z_1^0)^2\\ &\quad - \frac{a}{4}\langle y_2^2\rangle - \frac{a}{4}b_2\langle\varsigma_2^2\rangle + \frac{a}{4}(1-2z_2^0)\langle x_2 y_2\rangle + \frac{a}{4}b_2(z_2^0)^2.\end{aligned} \tag{20}$$

We emphasize that the derivation of (20) relies only on the temperature equations. Then (6) in the form $0 = \frac{2}{1+k^2}(-\mathrm{Pe}^2/\mathrm{Ra} + \mathrm{Nu} - 1)$

yields

$$0 = -\left(\frac{1}{r_1}\langle x_1^2\rangle + \frac{a}{4}\frac{1}{r_2}\langle x_2^2\rangle + \frac{1}{r_3}\langle w_1^2\rangle + \frac{1}{r_4}\langle w_2^2\rangle\right) + \langle x_1 y_1\rangle + \frac{a}{4}\langle x_2 y_2\rangle \tag{21}$$

where r_i (for $i = 1, 2, 3, 4$) are proportional to Ra and a rational function of k; see Appendix A. Adding (20) and (21) produces the expression

$$\begin{aligned} 0 = &- \langle y_1^2\rangle - b_1\langle \varsigma_1^2\rangle - \frac{a}{4}\langle y_2^2\rangle - \frac{a}{4}b_2\langle \varsigma_2^2\rangle \\ &+ 2(1 - z_1^0)\langle x_1 y_1\rangle + b_1(z_1^0)^2 - \frac{1}{r_1}\langle x_1^2\rangle \\ &+ 2\frac{a}{4}(1 - z_2^0)\langle x_2 y_2\rangle + \frac{a}{4}b_2(z_2^0)^2 - \frac{a}{4}\frac{1}{r_2}\langle x_2^2\rangle \\ &- \frac{1}{r_3}\langle x_3^2\rangle - \frac{1}{r_4}\langle x_4^2\rangle. \end{aligned} \tag{22}$$

Now introduce "balance parameter" α and add zero in the form $\alpha\times$ (22) to the right hand side of

$$\langle x_1 y_1\rangle + \frac{a}{4}\langle x_2 y_2\rangle = \frac{1}{r_1}\langle x_1^2\rangle + \frac{a}{4}\frac{1}{r_2}\langle x_2^2\rangle + \frac{1}{r_3}\langle w_1^2\rangle + \frac{1}{r_4}\langle w_2^2\rangle \tag{23}$$

to see that

$$\begin{aligned} &\langle x_1 y_1\rangle + \frac{a}{4}\langle x_2 y_2\rangle \\ &= \left\langle \begin{bmatrix} x_1 & y_1 \end{bmatrix} \begin{bmatrix} \frac{1}{r_1}(1-\alpha) & \alpha(1 - z_1^0) \\ \alpha(1 - z_1^0) & -\alpha \end{bmatrix} \begin{bmatrix} x_1 \\ y_1 \end{bmatrix} \right\rangle + b_1\alpha(z_1^0)^2 \\ &\quad + \frac{a}{4}\left\langle \begin{bmatrix} x_2 & y_2 \end{bmatrix} \begin{bmatrix} \frac{1}{r_2}(1-\alpha) & \alpha(1 - z_2^0) \\ \alpha(1 - z_2^0) & -\alpha \end{bmatrix} \begin{bmatrix} x_2 \\ y_2 \end{bmatrix} \right\rangle \\ &\quad + \frac{a}{4}b_2\alpha(z_2^0)^2 \\ &\quad - \alpha b_1\langle \varsigma_1^2\rangle - \alpha\frac{a}{4}b_2\langle \varsigma_2^2\rangle + \left(\frac{1-\alpha}{r_3}\right)\langle w_1^2\rangle \\ &\quad + \left(\frac{1-\alpha}{r_4}\right)\langle w_2^2\rangle. \end{aligned} \tag{24}$$

The essence of the background method is the observation that *if* we can choose $\alpha \in [1, \infty)$ and z_1^0 and z_2^0 so that the matrices in (24) are negative semi-definite, then we have produced an upper bound on $\frac{2}{1+k^2}(\mathrm{Nu} - 1)$ of the form

$$\langle x_1 y_1\rangle + \frac{a}{4}\langle x_2 y_2\rangle \le b_1\alpha(z_1^0)^2 + \frac{a}{4}b_2\alpha(z_2^0)^2. \tag{25}$$

For example choosing $z_1^0 = 0 = z_2^0$, it is easy to check that both matrices are negative semi-definite when $r_1 \le (\alpha - 1)/\alpha$. Thus $\mathrm{Nu} = 1$ is the upper bound for $\mathrm{Ra} \le (\alpha - 1)(1 + k^2)^3/\alpha k^2$ for any $\alpha \in [1, \infty)$. Taking the limit $\alpha \to \infty$, this shows that the $\mathrm{Nu} = 1$ conduction state is absolutely stable for all $\mathrm{Ra} < \mathrm{Ra}_c(k^2) \equiv (1 + k^2)^3/k^2$.

To deduce bounds for higher Rayleigh numbers ($r_1 > 1$), let $\alpha = \frac{z_1^0 + z_2^0}{(z_1^0)^2 + (z_2^0)^2}$; we will soon choose $z_1^0 \in (0, 1)$ and $z_2^0 \in [0, 1)$ so that $\alpha \in (1, \infty)$. Introduce

$$\rho_1 = \frac{(1 + k^2)^3}{k^2} \quad \text{and} \quad \rho_2 = \frac{(4 + k^2)^3}{k^2} \tag{26}$$

so that $r_i = \mathrm{Ra}/\rho_i$ for $i = 1, 2$ and let the background variables be

$$z_1^0 = \left(1 - \frac{\rho_1}{\mathrm{Ra}}\right) \quad \text{and} \quad z_2^0 = 0. \tag{27}$$

Then the matrices in (24) are both negative semi-definite for $\rho_1 < \mathrm{Ra} \le \sqrt{\rho_1\rho_2}$.

For $\mathrm{Ra} > \sqrt{\rho_1\rho_2}$ choose

$$z_1^0 = \sqrt{\rho_1}\frac{-\rho_1 + 2\mathrm{Ra}\sqrt{\frac{\rho_2}{\rho_1}} - \rho_2 + \sqrt{(\rho_1 + \rho_2)^2 + 4\mathrm{Ra}(\mathrm{Ra} - 2\sqrt{\rho_1\rho_2})}}{2\mathrm{Ra}(\sqrt{\rho_1} + \sqrt{\rho_2})},$$

$$z_2^0 = \sqrt{\frac{\rho_2}{\rho_1}}(z_1^0 - 1) + 1.$$

Then it is straightforward (albeit somewhat tedious) to confirm that $z_1^0, z_2^0 \in (0, 1)$ and the matrices are negative semi-definite when $\mathrm{Ra} > \sqrt{\rho_1\rho_2}$. Combining the results, the upper bounds are

$$\mathrm{Nu} \le \begin{cases} 1 & \text{for } \mathrm{Ra} \in [0, \rho_1) \\ 1 + 2\left(1 - \frac{\rho_1}{\mathrm{Ra}}\right) & \text{for } \mathrm{Ra} \in [\rho_1, \sqrt{\rho_1\rho_2}) \\ 1 + 2\left(1 - \frac{\rho_1}{\mathrm{Ra}}\right) + \frac{\rho_1 - \rho_2 + \sqrt{(\rho_2 - \rho_1)^2 + 4(\mathrm{Ra} - \sqrt{\rho_1\rho_2})^2}}{\mathrm{Ra}} & \text{for } \mathrm{Ra} \in [\sqrt{\rho_1\rho_2}, \infty). \end{cases} \tag{28}$$

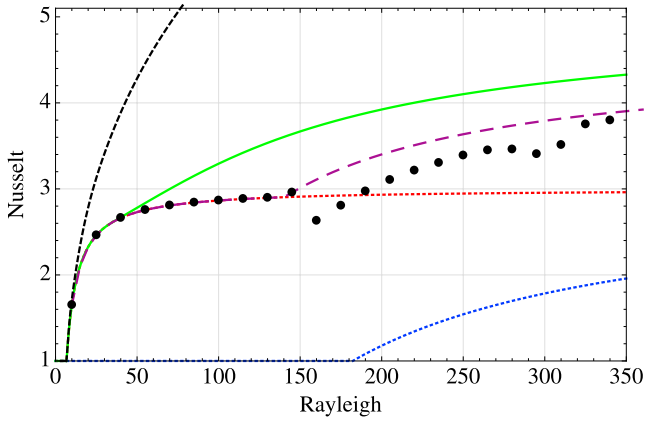

Fig. 1. (Color online) The top (black) dashed line is the best known upper bound for the full Rayleigh–Bénard problem from [16]. The solid (green) curve is the background method upper bound on all solutions of the Double Lorenz Equations. Rayleigh–Nusselt relations for several steady states are also shown. The dotted (red) curve asymptoting to $\mathrm{Nu} = 3$ is the steady solution of the first Lorenz system, and the lower dotted (blue) curve is the steady state of the second Lorenz system. The long-dashed (purple) curve is the steady state for the coupled system for $\sigma = 10$. The discrete dots are results from time averages of direct numerical simulations of the Double Lorenz Equations for $\sigma = 10$.

Fig. 1 is a plot of the bound, the steady state solutions, and results of some direct numerical simulations (dns) of the Double Lorenz Equations with aspect ratio $A = 2\sqrt{2}$ and Prandtl number $\sigma = 10$. For additional information the best known numerically computed upper bound (the black dashed line) for the PDE is included in the figure as well [16]. The dns data is generated using a finite time sample of a signal that is integrated for a long enough time interval to eliminate transients. It is computed using three different definitions of the Nusselt number (which are equivalent in the long time average) and are within one percent of one another for the finite time samples of the figure. Indeed, the Nusselt number has all of the following representations,

$$\mathrm{Nu} = 1 + \frac{1 + k^2}{2}\left\langle x_1 y_1 + \frac{a}{4}x_2 y_2\right\rangle,$$

$$\begin{aligned} \mathrm{Nu} &= 1 + \mathrm{Pe}^2/\mathrm{Ra} \\ &= 1 + \left(\frac{1}{r_1}\langle x_1^2\rangle + \frac{a}{4}\frac{1}{r_2}\langle x_2^2\rangle + \frac{1}{r_3}\langle w_1^2\rangle + \frac{1}{r_4}\langle w_2^2\rangle\right)\frac{1 + k^2}{2}, \end{aligned}$$

$$\mathrm{Nu} = 1 + 2\langle z_1 + z_2\rangle.$$

The bound is sharp – saturated by the nontrivial steady state – until $\mathrm{Ra} = 81\sqrt{3}/4 \approx 35$ (i.e., $\sqrt{\rho_1\rho_2}$ for this aspect ratio) but apparently not at higher Rayleigh numbers. The steady states appear to be stable until around $\mathrm{Ra} \approx 140$ at which point the solutions become time-dependent. The second drop in the numerically computed Nusselt number at around $\mathrm{Ra} \approx 290$ comes from a transition to seemingly periodic solutions. For this truncated system the Nusselt number bound asymptotes to $\mathrm{Nu} = 5$ as can be seen from (28) by taking the limit $\mathrm{Ra} \to \infty$.

As will be shown in the next section, the upper bound cannot be lowered by including more information from the equations of motion for the temperature variables. This does not preclude the possibility of lowering the bound by incorporating additional constraints via the velocity equations x_1, x_2, w_1 and w_2. In the background method the only place the velocity variables came into the background analysis is via the $\mathrm{Pe}^2 = \mathrm{Ra}\,(\mathrm{Nu} - 1)$ relation.

3. Optimal control analysis

We now provide a complementary analysis to bound heat transport in the Double Lorenz system. Instead of subjecting the velocity variables x_i, w_i to a momentum equation, we fix the total intensity of all the variables, the Péclet number (18), and attempt to deduce the optimal stirring strategy. Said differently, we treat the velocity field variables x_i and w_i for $i = 1, 2$ as control variables subject to the finite Péclet number condition. A global upper bound to this optimal control problem is an upper bound to heat transport in the Double Lorenz Equations with Ra defined by (6). This formulation has the additional benefit of producing flows for which the upper bound may be achieved, something that is lacking in the background method.

The optimal control problem is to maximize $\langle x_1 y_1 + \frac{a}{4} x_2 y_2 \rangle \equiv \frac{2}{1+k^2}(\mathrm{Nu} - 1)$ subject to

$$\dot{y}_1 = -y_1 + x_1 - x_1 z_1 + \frac{1}{2}(w_1 - w_2) y_2 \tag{29}$$

$$\dot{z}_1 = -b_1 z_1 + x_1 y_1 \tag{30}$$

$$\dot{y}_2 = -a y_2 + a x_2 - a x_2 z_2 - 2(w_1 - w_2) y_1 \tag{31}$$

$$\dot{z}_2 = -b_2 a z_2 + a x_2 y_2 \tag{32}$$

$$\mathrm{Pe}^2 = \left\langle 2\frac{\rho_1}{b_1} x_1^2 + 2\frac{\rho_2}{b_2} x_2^2 + \frac{\rho_1 b_1}{2}\left(w_1^2 + 9 w_2^2\right) \right\rangle, \tag{33}$$

where the expression for Péclet has been rewritten using the definitions of ρ_1, ρ_2, b_1, and b_2 in preparation for subsequent calculations (see Appendix A for the definitions of the constants). Equivalently, the functional to be extremized is

$$\begin{aligned}
\mathcal{F} = \Big\langle & \left(x_1 y_1 + \frac{a}{4} x_2 y_2\right) \\
& + \upsilon_1 \left(-y_1 + x_1 - x_1 z_1 + \frac{1}{2}(w_1 - w_2) y_2 - \dot{y}_1\right) \\
& - \zeta_1 (-b_1 z_1 + x_1 y_1 - \dot{z}_1) \\
& + \frac{1}{4}\upsilon_2 \left(-a y_2 + a x_2 - a x_2 z_2 - 2(w_1 - w_2) y_1 - \dot{y}_2\right) \\
& - \frac{1}{4}\zeta_2 \left(-b_2 a z_2 + a x_2 y_2 - \dot{z}_2\right) \\
& + \frac{\mu}{2}\left(\mathrm{Pe}^2 - \left[2\frac{\rho_1}{b_1} x_1^2 + 2\frac{\rho_2}{b_2} x_2^2 + \frac{\rho_1 b_1}{2}\left(w_1^2 + 9 w_2^2\right)\right]\right)\Big\rangle
\end{aligned} \tag{34}$$

where the Lagrange multipliers (a.k.a. adjoint variables) $\upsilon_i(t)$ and $\zeta_i(t)$ for $i = 1, 2$ enforce the temperature equations and μ enforces the finite Péclet number condition. The Euler–Lagrange equations for the extreme values are the temperature and adjoint variable differential equations

$$\dot{y}_1 = -y_1 + x_1 - x_1 z_1 + \frac{1}{2}(w_1 - w_2) y_2 \tag{35}$$

$$\dot{z}_1 = -b_1 z_1 + x_1 y_1 \tag{36}$$

$$\dot{\upsilon}_1 = \upsilon_1 - x_1 + x_1 \zeta_1 + \frac{1}{2}(w_1 - w_2)\upsilon_2 \tag{37}$$

$$\dot{\zeta}_1 = b_1 \zeta_1 - x_1 \upsilon_1 \tag{38}$$

$$\dot{y}_2 = -a y_2 + a x_2 - a x_2 z_2 - 2(w_1 - w_2) y_1 \tag{39}$$

$$\dot{z}_2 = -b_2 a z_2 + a x_2 y_2 \tag{40}$$

$$\dot{\upsilon}_2 = a\upsilon_2 - a x_2 + a x_2 \zeta_2 - 2(w_1 - w_2)\upsilon_1 \tag{41}$$

$$\dot{\zeta}_2 = b_2 \zeta_2 - x_2 \upsilon_2 \tag{42}$$

and the optimal stirring conditions

$$x_1 = \frac{1}{2\mu}\frac{b_1}{\rho_1}\left(\upsilon_1(1 - z_1) + y_1(1 - \zeta_1)\right) \tag{43}$$

$$x_2 = \frac{1}{2\mu}\frac{b_1}{\rho_2}\left(\upsilon_2(1 - z_2) + y_2(1 - \zeta_2)\right) \tag{44}$$

$$w_1 = \frac{1}{\mu}\frac{1}{\rho_1 b_1}\left(\upsilon_1 y_2 - \upsilon_2 y_1\right) \tag{45}$$

$$w_2 = -\frac{9}{\mu}\frac{1}{\rho_1 b_1}\left(\upsilon_1 y_2 - \upsilon_2 y_1\right) \tag{46}$$

$$\mathrm{Pe}^2 = \left\langle 2\frac{\rho_1}{b_1} x_1^2 + 2\frac{\rho_2}{b_2} x_2^2 + \frac{\rho_1 b_1}{2}\left(w_1^2 + 9 w_2^2\right)\right\rangle. \tag{47}$$

The identity $\frac{a}{4} b_2 = b_1$ was used in deriving the expression for x_2, a helpful simplification for later calculations. We refer to this entire system as the Optimal Double Lorenz Equations, and in the following analysis we prove that the global optimum upper bound on the Nusselt number is realized by a steady solution.

Some of the steady solutions to the Optimal Double Lorenz Equations for $\sqrt{\frac{1}{\mu}\frac{b_1}{\rho_2}} - 1 \geq 0$ are

$$y_i = \upsilon_i = b_i \frac{x_i}{b_i + (x_i)^2} \tag{48}$$

$$z_i = \zeta_i = \frac{(x_i)^2}{b_i + (x_i)^2} \tag{49}$$

$$(x_i)^2 = b_i\left(\sqrt{\frac{b_1}{\rho_i \mu}} - 1\right) \tag{50}$$

$$w_i = 0 \tag{51}$$

$$\mathrm{Pe}^2 = 2\sqrt{\frac{b_1}{\mu}}\left(\sqrt{\rho_1} + \sqrt{\rho_2}\right) - 2\rho_1 - 2\rho_2 \tag{52}$$

for $i = 1, 2$. If $\sqrt{\frac{1}{\mu}\frac{b_1}{\rho_2}} - 1 \leq 0$ and $\sqrt{\frac{1}{\mu}\frac{b_1}{\rho_1}} - 1 \geq 0$ then $0 = x_2 = y_2 = z_2 = \zeta_2 = \upsilon_2$, Eqs. (48) through (51) remain the same for $i = 1$, and $\mathrm{Pe}^2 = 2\left(\sqrt{\frac{\rho_1 b_1}{\mu}} - \rho_1\right)$. Lastly, if $\sqrt{\frac{1}{\mu}\frac{b_1}{\rho_1}} - 1 \leq 0$ then the only solution to the equations is zero. Eliminating μ in favor of Pe, reveals two exceptional Péclet regimes $0 \leq \mathrm{Pe}^2 \leq 2(\sqrt{\rho_1\rho_2} - \rho_1)$ and $\mathrm{Pe}^2 > 2(\sqrt{\rho_1\rho_2} - \rho_1)$. Of particular interest are the steady state solutions for z_1 and z_2 rewritten in terms of Péclet in the different regimes,

$$z_1 = \begin{cases} \dfrac{\mathrm{Pe}^2}{\mathrm{Pe}^2 + 2\rho_1} & \text{for } \mathrm{Pe}^2 \in [0, 2(\sqrt{\rho_1\rho_2} - \rho_1)] \\ \dfrac{\mathrm{Pe}^2 + 2(\rho_2 - \sqrt{\rho_1\rho_2})}{\mathrm{Pe}^2 + 2(\rho_1 + \rho_2)} & \text{for } \mathrm{Pe}^2 \in [2(\sqrt{\rho_1\rho_2} - \rho_1), \infty), \end{cases} \tag{53}$$

$$z_2 = \begin{cases} 0 & \text{for } \mathrm{Pe}^2 \in [0, 2(\sqrt{\rho_1\rho_2} - \rho_1)] \\ \dfrac{\mathrm{Pe}^2 + 2(\rho_1 - \sqrt{\rho_1\rho_2})}{\mathrm{Pe}^2 + 2(\rho_1 + \rho_2)} & \text{for } \mathrm{Pe}^2 \in [2(\sqrt{\rho_1\rho_2} - \rho_1), \infty). \end{cases} \tag{54}$$

Note that $\mathrm{Nu} = 1 + 2(z_1 + z_2)$ so the corresponding transport values are

$$\mathrm{Nu} = \begin{cases} 1 + 2\dfrac{\mathrm{Pe}^2}{\mathrm{Pe}^2 + 2\rho_1} & \text{for } \mathrm{Pe}^2 \in [0, 2(\sqrt{\rho_1\rho_2} - \rho_1)] \\ 1 + 4\dfrac{\mathrm{Pe}^2 + (\sqrt{\rho_2} - \sqrt{\rho_1})^2}{\mathrm{Pe}^2 + 2(\rho_1 + \rho_2)} & \text{for } \mathrm{Pe}^2 \in [2(\sqrt{\rho_1\rho_2} - \rho_1), \infty). \end{cases} \tag{55}$$

Using (6) to re-express (55) in terms of Ra we recover (28). That is, these steady states correspond precisely to the background bound.

We now show that the Nusselt number for any solution of the Optimal Double Lorenz Equations is bounded from above by steady solutions. To do so we will employ the background method yet again. The equations of motion for the momentum variables (x_i, w_i) for $i = 1, 2$ are no longer available, but we still have the evolution equations for the temperature variables y_i and z_i (for $i = 1, 2$) to work with, and the same background-type decomposition $z_i = \varsigma_i + z_i^0$ can be used.

Only the temperature equations were used to derive (20), so it still holds for the Optimal Double Lorenz system. Adding $\langle x_1 y_1\rangle + \frac{a}{4}\langle x_2 y_2\rangle$ to both sides of (20), and then adding zero in the form

$$0 = \alpha^2 \left(1 - \frac{\left\langle 2\frac{\rho_1}{b_1}x_1^2 + 2\frac{\rho_2}{b_2}x_2^2 + \frac{\rho_1 b_1}{2}\left(w_1^2 + 9w_2^2\right)\right\rangle}{\mathrm{Pe}^2}\right) \tag{56}$$

(where $\alpha^2 \geq 0$) to the right hand side of (20), it is evident that

$$\begin{aligned} &\langle x_1 y_1\rangle + \frac{a}{4}\langle x_2 y_2\rangle \\ &\quad = \alpha^2 + b_1 (z_1^0)^2 - \left\langle \begin{bmatrix} x_1 & y_1 \end{bmatrix} \begin{bmatrix} \dfrac{2\rho_1}{b_1 \mathrm{Pe}^2}\alpha^2 & z_1^0 - 1 \\ z_1^0 - 1 & 1 \end{bmatrix} \begin{bmatrix} x_1 \\ y_1 \end{bmatrix} \right\rangle \\ &\qquad - b_1\langle \varsigma_1^2\rangle - \frac{\alpha^2}{\mathrm{Pe}^2}\frac{\rho_1 b_1}{2}\langle w_1^2\rangle + \frac{a}{4} b_2 (z_2^0)^2 \\ &\qquad - \frac{a}{4}\left\langle \begin{bmatrix} x_2 & y_2 \end{bmatrix} \begin{bmatrix} \dfrac{2\rho_2}{b_1 \mathrm{Pe}^2}\alpha^2 & z_2^0 - 1 \\ z_2^0 - 1 & 1 \end{bmatrix} \begin{bmatrix} x_2 \\ y_2 \end{bmatrix} \right\rangle \\ &\qquad - \frac{a}{4} b_2 \langle \varsigma_2^2\rangle - \frac{\alpha^2}{\mathrm{Pe}^2}\frac{9\rho_1 b_1}{2}\langle w_2^2\rangle. \end{aligned} \tag{57}$$

The relation $\frac{a}{4} b_2 = b_1$ was used to rewrite the top left corner of the second matrix.

We must now choose the background and constant α^2. Let

$$\alpha^2 = b_1 (z_1^0 (1 - z_1^0) + z_2^0 (1 - z_2^0)). \tag{58}$$

For the $\mathrm{Pe}^2 \leq 2(\sqrt{\rho_1\rho_2} - \rho_1)$ regime pick the steady states

$$z_1^0 = \frac{\mathrm{Pe}^2}{\mathrm{Pe}^2 + 2\rho_1} \quad \text{and} \quad z_2^0 = 0 \tag{59}$$

and confirm that the second matrix in (57) is positive definite. Also, the relation

$$\frac{2\rho_1}{b_1}\frac{\alpha^2}{\mathrm{Pe}^2} = (1 - z_1^0)^2 \tag{60}$$

holds allowing us to rewrite (57) in the $\mathrm{Pe}^2 \leq 2(\sqrt{\rho_1\rho_2} - \rho_1)$ regime as

$$\begin{aligned} &\langle x_1 y_1\rangle + \frac{a}{4}\langle x_2 y_2\rangle \\ &\quad = b_1 \frac{\mathrm{Pe}^2}{\mathrm{Pe}^2 + 2\rho_1} - \langle (x_1 (z_1^0 - 1) + y_1)^2\rangle - b_1\langle \varsigma_1^2\rangle \\ &\qquad - \frac{a}{4}\langle (x_2 - y_2)^2\rangle - \frac{a}{4}\left(\frac{4\rho_1\rho_2}{(\mathrm{Pe}^2 + 2\rho_1)^2} - 1\right)\langle x_2^2\rangle - \frac{a}{4} b_2 \langle \varsigma_2^2\rangle \\ &\qquad - \frac{\alpha^2}{\mathrm{Pe}^2}\frac{\rho_1 b_1}{2}(\langle w_1^2\rangle + 9\langle w_2^2\rangle). \end{aligned} \tag{61}$$

This expression implies that $b_1 \frac{\mathrm{Pe}^2}{\mathrm{Pe}^2 + 2\rho_1}$ is an upper bound since all the subsequent terms are negative. An examination of (55) reveals a correspondence to a steady state Nusselt number.

For the $\mathrm{Pe}^2 > 2(\sqrt{\rho_1\rho_2} - \rho_1)$ regime we again pick steady state solutions for z_i for the backgrounds, namely,

$$\begin{aligned} z_1^0 &= \frac{\mathrm{Pe}^2 + 2(\rho_2 - \sqrt{\rho_1\rho_2})}{\mathrm{Pe}^2 + 2(\rho_1 + \rho_2)} \quad \text{and} \\ z_2^0 &= \frac{\mathrm{Pe}^2 + 2(\rho_1 - \sqrt{\rho_1\rho_2})}{\mathrm{Pe}^2 + 2(\rho_1 + \rho_2)}. \end{aligned} \tag{62}$$

Observe that

$$1 - z_1^0 = 2\frac{\rho_1 + \sqrt{\rho_1\rho_2}}{\mathrm{Pe}^2 + 2(\rho_1 + \rho_2)} = 2\sqrt{\rho_1}\frac{\sqrt{\rho_1} + \sqrt{\rho_2}}{\mathrm{Pe}^2 + 2(\rho_1 + \rho_2)}, \tag{63}$$

$$1 - z_2^0 = 2\frac{\rho_2 + \sqrt{\rho_1\rho_2}}{\mathrm{Pe}^2 + 2(\rho_1 + \rho_2)} = 2\sqrt{\rho_2}\frac{\sqrt{\rho_1} + \sqrt{\rho_2}}{\mathrm{Pe}^2 + 2(\rho_1 + \rho_2)}, \tag{64}$$

$$\alpha^2 = b_1 2\frac{\mathrm{Pe}^2\left(\sqrt{\rho_1} + \sqrt{\rho_2}\right)^2}{(\mathrm{Pe}^2 + 2(\rho_1 + \rho_2))^2}, \tag{65}$$

hence the top left corners of the matrices in (57) are simplified to

$$\frac{2\rho_1}{b_1}\frac{\alpha^2}{\mathrm{Pe}^2} = 4\rho_1\frac{\left(\sqrt{\rho_1} + \sqrt{\rho_2}\right)^2}{(\mathrm{Pe}^2 + 2(\rho_1 + \rho_2))^2} = (1 - z_1^0)^2, \tag{66}$$

$$\frac{2\rho_2}{b_1}\frac{\alpha^2}{\mathrm{Pe}^2} = 4\rho_2\frac{\left(\sqrt{\rho_1} + \sqrt{\rho_2}\right)^2}{(\mathrm{Pe}^2 + 2(\rho_1 + \rho_2))^2} = (1 - z_2^0)^2. \tag{67}$$

With these facts in place rewrite (57) as

$$\begin{aligned} \langle x_1 y_1\rangle + \frac{a}{4}\langle x_2 y_2\rangle =& 2b_1\frac{\mathrm{Pe}^2 + (\sqrt{\rho_2} - \sqrt{\rho_1})^2}{\mathrm{Pe}^2 + 2(\rho_1 + \rho_2)} \\ &- \langle (x_1 (z_1^0 - 1) + y_1)^2\rangle - b_1\langle \varsigma_1^2\rangle \\ &- \frac{a}{4}\langle (x_2 (z_2^0 - 1) + y_2)^2\rangle - \frac{a}{4} b_2 \langle \varsigma_2^2\rangle \\ &- \frac{\alpha^2}{\mathrm{Pe}^2}\frac{\rho_1 b_1}{2}(\langle w_1^2\rangle + 9\langle w_2^2\rangle). \end{aligned} \tag{68}$$

All the terms following $2b_1\frac{\mathrm{Pe}^2 + (\sqrt{\rho_2} - \sqrt{\rho_1})^2}{\mathrm{Pe}^2 + 2(\rho_1 + \rho_2)}$ are negative and again we have a correspondence to a steady state Nusselt number in (55). This establishes that the absolute maximum value is realized by the optimal steady state stirring, i.e., for any extremum of $\mathcal{F}$ we have

$$\mathrm{Nu} \leq \begin{cases} 1 + 2\dfrac{\mathrm{Pe}^2}{\mathrm{Pe}^2 + 2\rho_1} & \text{for } \mathrm{Pe}^2 \in [0, 2(\sqrt{\rho_1\rho_2} - \rho_1)], \\ 1 + 4\dfrac{\mathrm{Pe}^2 + (\sqrt{\rho_2} - \sqrt{\rho_1})^2}{\mathrm{Pe}^2 + 2(\rho_1 + \rho_2)} & \text{for } \mathrm{Pe}^2 \in [2(\sqrt{\rho_1\rho_2} - \rho_1), \infty). \end{cases} \tag{69}$$

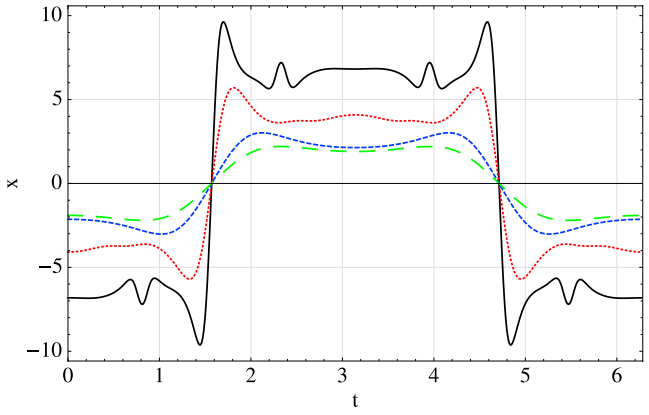

Fig. 2. (Color online) Time dependence of optimal 2π (time) periodic stirring protocols for several value of the Péclet number and $k = 1/\sqrt{2}$. Here we show $x_1(t)$. Long dashed (green) line: Pe = 4.2; short dashed (blue) line: Pe = 5.4; dotted (red) line Pe = 14.1; and solid (black) curve: Pe = 35.1.

3.1. Comparison of steady state to periodic solutions

Eqs. (61) and (68) show that the only periodic solutions that saturate the upper bound are the steady. Indeed, in the $\mathrm{Pe}^2 \leq 2(\sqrt{\rho_1\rho_2} - \rho_1)$ regime if equality holds in (69) then it must be the case that $w_i = \zeta_i = 0$ for $i = 1, 2, x_1(1 - z_1) = y_1, x_2 = y_2$. This means that z_i is constant; it is equal to the background. Using the y_i equations and the relations $x_1(1 - z_1) = y_1$ and $x_2 = y_2$, we can conclude that $\dot{y}_i = 0$ and that $x_2 = y_2 = z_2 = 0$. Similar reasoning leads to the same conclusion about the optimizer for $\mathrm{Pe}^2 \geq 2(\sqrt{\rho_1\rho_2} - \rho_1)$.

It is interesting to examine why the periodic solutions do worse than the steady state. We have computed time-dependent periodic solutions to the Optimal Double Lorenz system using standard methods: a Fourier Galerkin truncation, Newton–Kantorovich iteration, and numerical continuation. This is the same method that was used in [15]. In Fig. 2 we show the solutions for $x_1(t)$ for several different Péclet number. As the Péclet number is increased the solutions begin to develop sharp transition regions from positive/negative steady states. That is, it appears that the controls "want" to remain steady, but are unable to do so due to the branch that they were numerically continued from.

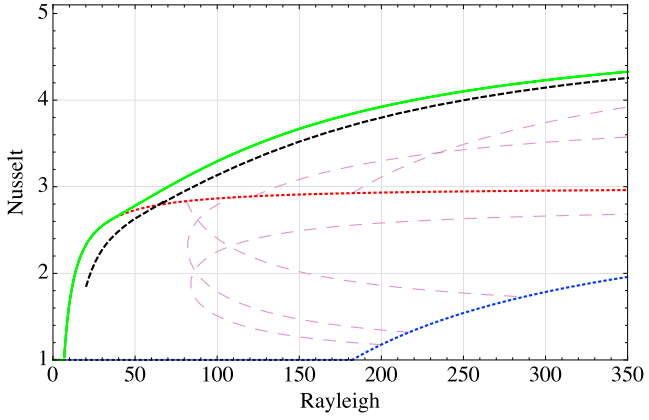

Fig. 3. (Color online) The top (green) curve is the upper bound on the Nusselt number. Rayleigh–Nusselt relations for several steady states of the Double Lorenz Equations are also shown. The long-dashed (purple) purple lines are the coupled steady state solutions for several Prandtl numbers, $\sigma = 0.44$ (bottom), 0.70, 1.42, 5.75 and 10^4 (top), and wavenumber is $k = 1/\sqrt{2}$. The upper dotted (red) curve is the first Lorenz system steady state while the lower dotted (blue) curve is that for the second Lorenz system. The dashed (black) line is the transport for a time-periodic solution to the optimal Double Lorenz system.

This is exactly analogous to what happens in the optimal control version of the (single) Lorenz system [15], where the transition between steady states control values is even simpler, absent some of the "ringing" that is seen in Fig. 2. The forced transitions in the time-dependent, albeit locally optimal, control have a cost in terms of the transport: it is definitely below the transport that is achieved by steady flow variables. Fig. 3 is a plot of the Nusselt number for some locally-optimal time-periodic controls and the steady state controls for the Optimal Double Lorenz Equations, along with some steady states of the Double Lorenz Equations at a selection of Prandtl numbers.

4. Discussion and summary

The apparent inability of both the background method and the optimal control problem to produce sharp upper bounds past $\mathrm{Ra} = \sqrt{\rho_1\rho_2}$ deserves some comment. It is possible that unstable time-dependent solutions to the Double Lorenz system saturate the upper bound, but we do not expect this to be the case. In the double Lorenz model the only way to activate both Lorenz modes at the same time ((x_i, y_i, z_i) for $i = 1, 2$) and hence have enhanced heat transport is to also have non-zero shear modes (w_i for $i = 1, 2$). That is to say if $w_1 = 0$ or $w_2 = 0$ then the equations of motion imply that either the first Lorenz mode is zero or the second. These shear modes do not contribute to heat transport and thus, as far as the optimal control problem or the background method is concerned, are ineffectual. The optimal control problem may choose to ignore these modes and achieve the same Nusselt number at a reduced Péclet cost. It seems that the only way to lower the bound is to either incorporate a shear mode constraint (or an advective constraint) into the optimal control formulation or perhaps a more judicious combination of moments from the equations of motion in the background method. The advective term of the velocity equations in the PDE is notoriously difficult to deal with and the goal of the optimal control formulation is precisely to bypass this barrier. Thus for the optimal control problem considered here incorporating additional constraints on the velocity variables detaches us from the original PDE optimal control problem.

In this work we investigated a truncated version of Rayleigh's model of thermal convection of a fluid heat from below using a combination of numerical and analytical techniques, producing rigorous upper bounds via the background method and a new optimal control formulation. The optimal control problems consist of maximizing the Nusselt number subject to incompressibility, the advection–diffusion equation, and an enstrophy amplitude condition. We obtained analytic steady-state solutions, numerical time-dependent periodic solutions, and rigorous bounds on heat transport for these systems. The bound is not saturated by steady or, apparently, time-dependent solutions of the Double Lorenz Equations, but they are realized as a fixed point of the Optimal Double Lorenz system. The eight mode model considered here suggests that steady solutions of the full optimal system produce the largest heat transport. This, in turn, indicates that the results of the optimal transport analysis for the full partial differential equations in Hassanzadeh et al. [17], which were limited to time-independent controls, may be more general than presumed.

Acknowledgments

The authors thank D. Goluskin for helpful discussions. This research was supported by the US National Science Foundation (NSF) Mathematical Physics award PHY-1205219 with an Alliances for Graduate Education and the Professoriate (AGEP) Graduate Research Supplement. We gratefully acknowledge the hospitality of Woods Hole Oceanographic Institution's *Geophysical Fluid*

Dynamics program (supported in part by NSF award OCE-1332750) and the *Mathematics of Turbulence* program at NSF's Institute for Pure & Applied Mathematics (located on the campus of the University of California, Los Angeles), where some of this work was completed.

Appendix A. Dictionary of coefficients and parameters

The constants in this paper are as follows:

$$\mathrm{Ra} = \text{ The Rayleigh number} \tag{A.1}$$
$$\mathrm{Nu} = \text{ The Nusselt number} \tag{A.2}$$
$$\sigma = \text{ Prandtl number} \tag{A.3}$$
$$A = \text{ Aspect Ratio} \tag{A.4}$$
$$k = 2/A \tag{A.5}$$
$$\rho_1 = \frac{(1+k^2)^3}{k^2} \tag{A.6}$$
$$\rho_2 = \frac{(4+k^2)^3}{k^2} \tag{A.7}$$
$$c_1 = \frac{(3+k^2)(4+k^2)}{2(1+k^2)^2} \tag{A.8}$$
$$d_1 = \frac{(4+k^2)(k^2-5)}{2(1+k^2)^2} \tag{A.9}$$
$$c_2 = \frac{2k^2(1+k^2)^2}{(4+k^2)^3} \tag{A.10}$$
$$d_2 = \frac{2(1+k^2)^2(k^2-8)}{(4+k^2)^3} \tag{A.11}$$
$$a = \frac{4+k^2}{1+k^2} \tag{A.12}$$
$$b_1 = \frac{4}{1+k^2} \tag{A.13}$$
$$b_2 = \frac{16}{4+k^2} \tag{A.14}$$
$$r_1 = \frac{\mathrm{Ra}}{\rho_1} \tag{A.15}$$
$$r_2 = \frac{\mathrm{Ra}}{\rho_2} \tag{A.16}$$
$$r_3 = \frac{k^2 b_1}{16}\mathrm{Ra} \tag{A.17}$$
$$r_4 = \frac{k^2 b_1}{128}\mathrm{Ra}. \tag{A.18}$$

We use the relations

$$\frac{2\rho_1}{b_1}c_1 - \frac{2\rho_2}{b_2}c_2 - \frac{3}{4}a\rho_1 = 0 \tag{A.19}$$
$$-\frac{2\rho_1}{b_1}d_1 + \frac{2\rho_2}{b_2}d_2 + \frac{3}{4}a\rho_1 = 0 \tag{A.20}$$

to derive (6) for the truncated system.

Appendix B. Dictionary of bounds

Consider the energy function

$$E(y_1, z_1, y_2, z_2) = \tfrac{1}{2}\left(y_1^2 + (z_1-1)^2 + \tfrac{1}{4}\left[y_2^2 + (z_2-1)^2\right]\right). \tag{B.1}$$

Taking the time derivative and making use of the temperature variable equations (10), (11), (13), and (14) yields

$$\dot{E}(y_1, z_1, y_2, z_2) = -y_1^2 - b_1 z_1^2 + b_1 z_1 + \frac{a}{4}\left(-y_2^2 - b_2 z_2^2 + b_2 z_2\right). \tag{B.2}$$

Adding zero in the form $2\alpha(E-E)$ where $\alpha \in (0, \min\{1, b_1\})$ to the right hand side of (B.2) results in the following differential inequality,

$$\begin{aligned}
&\dot{E}(y_1, z_1, y_2, z_2) \\
&\quad = -2\alpha E + \frac{5}{4}\alpha + (\alpha-1)y_1^2 + (\alpha-b_1)z_1^2 + (b_1-2\alpha)z_1 \\
&\qquad + \frac{1}{4}\left[(\alpha-a)y_2^2 + (\alpha-ab_2)z_2^2 + (ab_2-2\alpha)z_2\right] \\
&\quad = -2\alpha E + \frac{5}{4}\alpha + \frac{(b_1-2\alpha)^2}{4(b_1-\alpha)} + \frac{(ab_2-2\alpha)^2}{16(ab_2-\alpha)} \\
&\qquad + (\alpha-1)y_1 + (\alpha-b_1)\left(z_1 + \frac{b_1-2\alpha}{2(\alpha-b_1)}\right)^2 \\
&\qquad + \frac{\alpha-a}{4}y_2 + \frac{\alpha-ab_2}{4}\left(z_2 + \frac{ab_2-2\alpha}{2(\alpha-ab_2)}\right)^2 \\
&\quad \le -2\alpha E + \frac{b_1^2}{4(b_1-\alpha)} + \frac{b_1^2}{(4b_1-\alpha)}.
\end{aligned} \tag{B.3}$$

The differential inequality may be solved to yield

$$\begin{aligned}
E(t) \le & e^{-2\alpha t}\left(E_0 - \frac{1}{2\alpha}\left[\frac{b_1^2}{4(b_1-\alpha)} + \frac{b_1^2}{(4b_1-\alpha)}\right]\right) \\
& + \frac{1}{2\alpha}\left[\frac{b_1^2}{4(b_1-\alpha)} + \frac{b_1^2}{(4b_1-\alpha)}\right]
\end{aligned} \tag{B.4}$$

where E_0 is the initial value of the energy (B.2). The $\alpha \in (0, \min\{1, b_1\}]$ that minimizes the steady state of (B.4) is not terribly illuminating (it is the root of a cubic), thus we will instead pick the simpler but suboptimal $\alpha = b_1/2$ for $b_1 \in (0, 2]$ and $\alpha = 1$ for $b_1 \in (2, \infty)$ to explicitly display the time-asymptotic bounds

$$\begin{aligned}
&\limsup_{t\to\infty} E(y_1, z_1, y_2, z_2) \\
&\quad \le \begin{cases} \dfrac{9}{14} & \text{for } b_1 \in (0, 2) \\ \dfrac{1}{2}\left[\dfrac{b_1^2}{4(b_1-1)} + \dfrac{b_1^2}{(4b_1-1)}\right] & \text{for } b_1 \in [2, \infty) \end{cases}
\end{aligned} \tag{B.5}$$

on the temperature variables.

References

[1] H. Bénard, Toubillons cellulaires dans une nappe liquide, Rev. Gén. Sci. Pures Appl. 11 (1900) 1261–1328.
[2] Lord Rayleigh, On convection currents in a horizontal layer of fluid, when the higher temperature is on the under side, Phil. Mag. 32 (1916) 529–546.
[3] E.N. Lorenz, Deterministic nonperiodic flow, J. Atmospheric Sci. 20 (1963) 130–141.
[4] Y.M. Treve, O.P. Manley, Energy conserving Galerkin approximations for 2-D hydrodynamic and MHD Bénard convection, Physica D 4 (1982) 319–342.
[5] J. Thiffeault, W. Horton, Energy-conserving truncations for convection with shear flow, Phys. Fluids (1996) 1715–1719.
[6] A. Gluhovsky, C. Tong, E. Agee, Selection of modes in convective low-order models, J. Atmospheric Sci. 59 (2002) 1383–1393.
[7] D. Goluskin, Zonal flow driven by convection and convection driven by internal heating (Doctoral thesis), Columbia University, 2012, pp. 46–66.
[8] L.N. Howard, Heat transport by turbulent convection, J. Fluid Mech. 17 (1963) 405–432.
[9] F. Busse, On Howard's bound for heat transport by turbulent convection, J. Fluid Mech. 37 (1969) 457–477.
[10] C.R. Doering, P. Constantin, Variational bounds on energy dissipation in incompressible flows. III. Convection, Phys. Rev. E 53 (1996) 5957–5981.
[11] R.R. Kerswell, Unification of variational principles for turbulent shear flows: The background method of Doering-Constantin and the mean-fluctuation formulation of Howard-Busse, Physica D 121 (1998) 175–192.

[12] C.R. Doering, F. Otto, M.G. Reznikoff, Bounds on vertical heat transport for infinite-Prandtl-number Rayleigh-Bénard convection, J. Fluid Mech. 560 (2006) 229–241.
[13] J.P. Whitehead, C.R. Doering, Ultimate state of two-dimensional Rayleigh-Bénard convection between free-slip fixed-temperature boundaries, Phys. Rev. Lett. 106 (2011) 244501.
[14] F. Pétrélis, N. Pétrélis, Bounds on the dissipation in the Lorenz system, Phys. Lett. A 326 (2004) 85–92.
[15] A.N. Souza, C.R. Doering, Maximal transport in the Lorenz equations, Phys. Lett. A 379 (2015) 518–523.
[16] B. Wen, G.P. Chini, R.R. Kerswell, C.R. Doering, Aspect-ratio-dependent upper bounds for two-dimensional Rayleigh–Bénard convection between stress-free isothermal boundaries, Phys. Rev. E (2015) submitted for publication.
[17] P. Hassanzadeh, G.P. Chini, C.R. Doering, Wall to wall optimal transport, J. Fluid Mech. 751 (2014) 627–662.